J Appl Electrochem (2010) 40:285–293
DOI 10.1007/s10800-009-9972-5

ORIGINAL PAPER

Evaluation of corrosion behavior of surface modified Ti–6Al–4V ELI alloy in hanks solution

S. Tamilselvi · V. Raman · N. Rajendran

Received: 24 September 2008 / Accepted: 17 August 2009 / Published online: 3 September 2009

Abstract The passive film behavior of Ti–6Al–4V ELI (Extra Low Interstitial) alloy after a chemical treatment followed by a thermal treatment was morphologically and electrochemically characterized. The surface morphological studies were carried out using scanning electron microscopy (SEM), electron dispersive X-ray analysis (EDAX), and Fourier Transformed-Infra Red (FT-IR) analysis to investigate the nucleation and growth of apatite on the chemically and thermally treated Ti–6Al–4V ELI alloy immersed for different durations in Hanks solution. Polarization and impedance spectroscopic (EIS) measurements were carried out in Hanks solution and the electrical parameters were obtained for the passive film using a non-linear least square fitting (NLLS) method.

Keywords Alkali treatment · Corrosion · Electrochemical impedance spectroscopy · Scanning electron microscopy · Titanium alloys

1 Introduction

Titanium and its alloys have been widely used in dental and orthopedic prostheses, pacemakers, and heart valves [1]. The success of titanium-based materials in these applications is due to their excellent mechanical properties, good corrosion resistance, and biocompatibility [2]. The high corrosion resistance of titanium in various test solutions such as Ringer [3], saline [4], saliva [5], and other physiological media [6] is due to the formation of a protective oxide layer on its surface. However, the interaction between the metallic implant and the living tissue does not involve a chemical bond with bone. The lack of ability to bond chemically may lead to slow fixation of titanium alloys and to their gradual loosening over a long period.

Since last decade, different surface modifications have been employed to provide these implants with bone-bonding ability. These surface modifications mainly consists of physical coating processes on the metals involving ceramic materials, such as Bioglass® [7], Cerabone®, and A/W glass–ceramic [8]etc. Titanium implants, which must work as load-bearing parts, are commonly coated with a plasma-sprayed hydroxyapatite layer so as to make the surface bioactive [9]. However, the plasma-spray technique does not permit accurate control of the chemical composition, crystallographic structure, and crystallinity of the coating. As a result, the hydroxyapatite layer is mechanically and chemically unstable [10].

Recently, the method of inducing bioactivity for direct bone bonding with the implant by means of chemical surface modification on the biomaterial have been widely studied. Ohtsuki et al. [11] reported the bioactivity of H_2O_2-treated titanium and Li et al. [12] reported the TiO_2 synthesized by sol–gel method. Wen et al. [13] reported on the bioactivity of Ti alloy a by two-step chemical treatment by a combination of acid ($HCl + H_2SO_4$) followed by alkali. Kokubo and Kim [14] introduced alkali and heat treatments as a method of surface modification for titanium alloys to improve bioactivity. The alkali method treatment introduced by Kokubo has since then gathered interest. The morphological characterizations of alkali-treated titanium

S. Tamilselvi · V. Raman · N. Rajendran (✉)
Department of Chemistry, Anna University, Chennai, Chennai 600 025, India
e-mail: nrajendran@annauniv.edu

S. Tamilselvi
e-mail: salem_selvi@yahoo.com

V. Raman
e-mail: vraman78@yahoo.com

are well documented [15–23], whereas, only a few reports are available on the electrochemical characterization. Tamilselvi et al. [24] reported the corrosion behavior of untreated titanium alloys in SBF solution. However, attempts on the corrosion behavior of alkali and alkali heat-treated titanium alloys are yet to be reported. Hence, in the present study, the aim was to electrochemically assess the corrosion behavior of treated Ti–6Al–4V ELI alloy in Hanks solution using polarization and electrochemical impedance spectroscopy. Further, the surface characterization of alkali-treated (AT) and alkali heat-treated (AHT) Ti–6Al–4V ELI alloy immersed in Hanks solution was carried out using SEM-EDAX and FTIR analysis.

2 Methods and materials

2.1 Specimen preparation

The alloy Ti–6Al–4V ELI was used as the specimen (1 cm^2) and they were polished on one side using silicon carbide waterproof papers from 220, 400, 600, 800, 1000, 1200, 2000, and 2500 grit. Final polishing was done using 1 μm diamond paste in order to produce a scratch-free and mirror-finish surface. The polished specimens were washed with detergent solution, degreased with acetone and thoroughly washed with distilled water. This was followed by ultrasonic cleaning in acetone for 10 min and finally, the specimen was rinsed in distilled water and dried.

2.2 Surface treatment

Chemical treatment was performed by soaking the specimens in 5 mL of 10 M NaOH aqueous solution at 60 °C for 24 h, and then they were gently washed with distilled water and dried at 40 °C for 24 h in an air atmosphere. The subsequent thermal treatment was done by placing Ti–6Al–4V ELI alloy specimen in an aluminum boat heated at 600 °C for 1 h in an electric furnace and allowed to cool till room temperature before removing the specimen from the furnace.

2.3 Hanks solution

The Hanks solution was prepared by dissolving the reagents of composition (g/L) 8.00 NaCl, 0.35 $NaHCO_3$, 0.40 KCl, 0.06 KH_2PO_4, 0.48 $Na_2HPO_4{\cdot}2H_2O$, 0.10 $MgCl_2{\cdot}6H_2O$, 0.18 $CaCl_2$, 0.10 $MgSO_4{\cdot}7H_2O$, and 1.00 glucose into distilled water and the pH was adjusted to 7.4 with tris(hydroxymethyl) amminomethane ($(CH_2OH)_3$ (NH_3)) and hydrochloric acid at 36.5 °C. Each specimen was soaked in 25 mL of Hanks solution for different durations (0, 3, 5, 7, 10, 14, and 15 days). Then, the specimens were removed from Hanks solution, washed with distilled water and dried at room temperature.

2.4 Morphological characterization

The surface morphology of the specimens was analyzed using scanning electron microscope (SEM) after immersion in Hanks solution. SEM images were taken for untreated, alkali, and alkali heat-treated samples, using the instrument; JSM-840A, JOEL-Japan, Link ISIS, Oxford instrument UK, in combination with an energy dispersive X-ray analysis (EDAX). The specimens were carefully scratched and the resulting powder was mixed with KBr and pressed to form a pellet. This pellet was analyzed using FT-IR model Perkin-Elmer, USA ranging from 400–4,000 cm^{-1} to determine the functional groups.

2.5 Electrochemical characterization

The cell used for electrochemical studies consisted of a platinum electrode as the counter electrode, saturated calomel electrode as the reference electrode, and Ti–6Al–4V ELI alloy as working electrode with a surface area of 1 cm^2. Potentiodynamic polarization studies were carried out for alkali-treated (AT) and alkali heat-treated (AHT) Ti–6Al–4V ELI alloy immersed in Hanks solution. All the potential measurements were carried out at a scan rate of 1 mV/s between −1 and +2 V in an aerated medium. Potentiostat (model PGSTAT 12 with FRA, Autolab, The Netherlands B.V.) controlled by a personnel computer with dedicated software viz., General Purpose Electrochemical System (GPES version 6.0) was used for conducting the polarization experiments. In order to obtain reliable results, polarization experiments were triplicated in Hanks solution.

EIS studies were carried out using an electrochemical system frequency response analyzer (FRA), which included a potentiostat model PGSTAT 12. The impedance spectra were acquired in the frequency range of 10^4–10^{-2} Hz with a 10 mV amplitude sine wave generated by FRA. The impedance spectra (Nyquist and Bode plots) obtained for AT and AHT specimens in Hanks solution were fitted using a non-linear least square (NLLS) method.

3 Results and discussion

3.1 SEM–EDAX analysis

Figure 1a shows the SEM and EDAX results of untreated (UT) Ti–6Al–4V ELI alloy. The SEM micrographs exhibited a smooth surface and the EDAX results revealed well-defined peaks corresponding to Ti, Al, and V.

However, after the alkali treatment the surface morphology changed. Figure 1b shows the SEM and EDAX results of AT Ti–6Al–4V ELI alloy, which exhibited the formation of a porous network structure on the surface of the substrate. The EDAX results indicated the presence of Ti, Al, and V in the alloy along with Na. Further, on heat treatment at 600 °C, the porous structure densified as seen in Fig. 1c. EDAX results of AHT specimen revealed the presence of

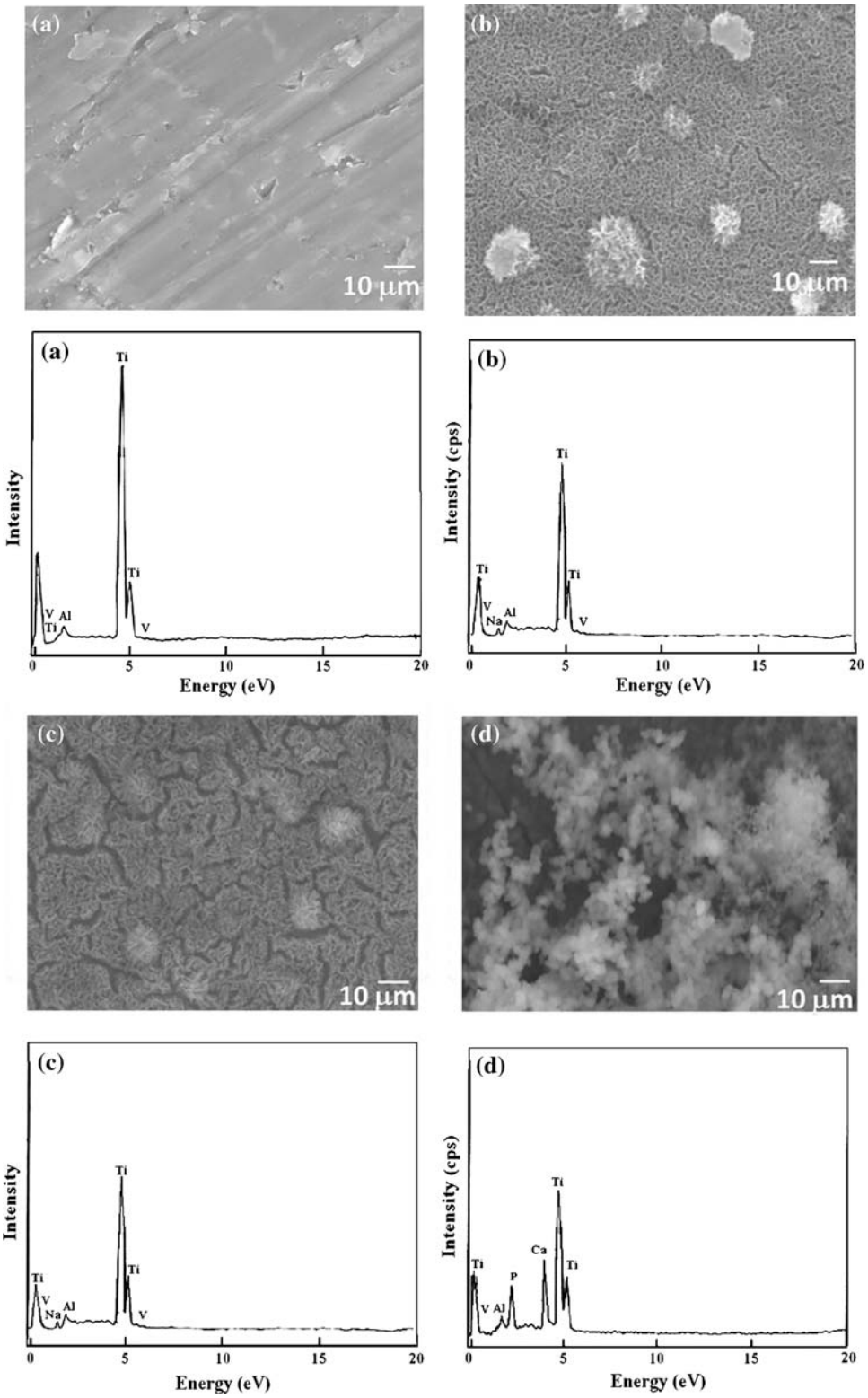

Fig. 1 SEM–EDAX analysis of Ti–6Al–4V ELI alloy **a** UT, **b** AT, **c** AHT, and **d** AHT after optimum period of immersion in Hanks solution

Ti, Al, and Na peaks. However, the intensity of the Ti and Na peaks were found to be diminished.

Figure 1d shows the SEM and EDAX results of the AHT specimen immersed in Hanks solution. Similar SEM and EDAX results were obtained for all the treated specimens after immersion in Hanks solution for optimum duration. The optimum immersion periods for all the treated samples were determined by analyzing the sample at regular intervals using SEM. However, only the results of AHT specimen immersed in Hanks solution for optimum duration is provided in this article in order to reduce the redundancy of the information. The SEM micrograph exhibited large globular particles on the AHT specimen and the EDAX results showed prominent Ca and P peaks.

Further, it was also observed that the globular particles were formed over UT, AT, and AHT specimens only after an optimum period of immersion in Hanks solution and this optimum period varied for each treatment method. Hence, it could be understood that a layer of apatite is formed over the surface only after a prolonged interaction of the Hanks solution with the porous network formed by alkali treatment [25].

In order to confirm the newly formed apatite layer over the untreated and treated surface, FT-IR analysis was carried out and results were given in Fig. 2. The main absorption bands at 1,470 and 1,640 cm^{-1} were assigned to C–O of the CO_3 group. The absorption bands at 1,074 and 587 cm^{-1} were assigned to P–O of the PO_4 group. The P–OH stretching of the HPO_4 group was observed at 873 cm^{-1}. The broad bands at 3,448 cm^{-1} due to adsorbed H_2O in the material and two broad bands at 2,369 and 2,345 cm^{-1} for soluble CO_2 were also observed. Similar results were reported for the FT-IR analysis of apatite [26–28]. From the above observations, it could be confirmed that a layer of apatite forms after immersion in Hanks solution [29].

3.2 Electrochemical corrosion studies

The surface treatments have profound effect on the electrochemical behavior during the immersion in Hanks solution. In order to understand the electrochemical changes during the immersion in Hanks solution, the AT and AHT Ti–6Al–4V ELI specimens were subjected to polarization and electrochemical impedance spectroscopic (EIS) studies.

3.2.1 Potentiodynamic polarization studies

The potentiodynamic polarization studies were carried out for the AT and AHT specimens, immediately and after optimum period of immersion in Hanks solution and the results are shown in Fig. 3a, b.

Figure 3a shows the polarization curves of AT specimen for immediate and optimum day (10th) of immersion in

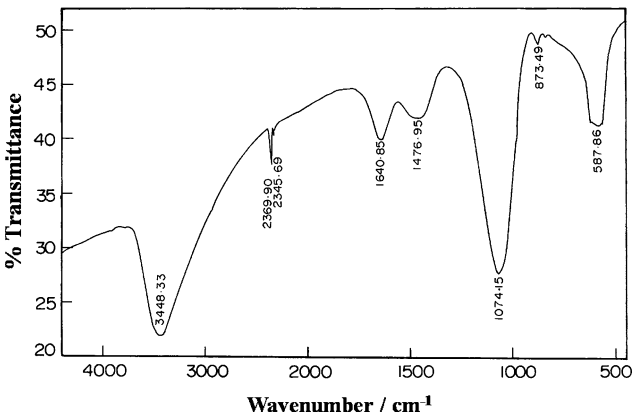

Fig. 2 FT-IR analysis of AHT Ti–6Al–4V ELI alloy immersed in Hanks solution for optimum days

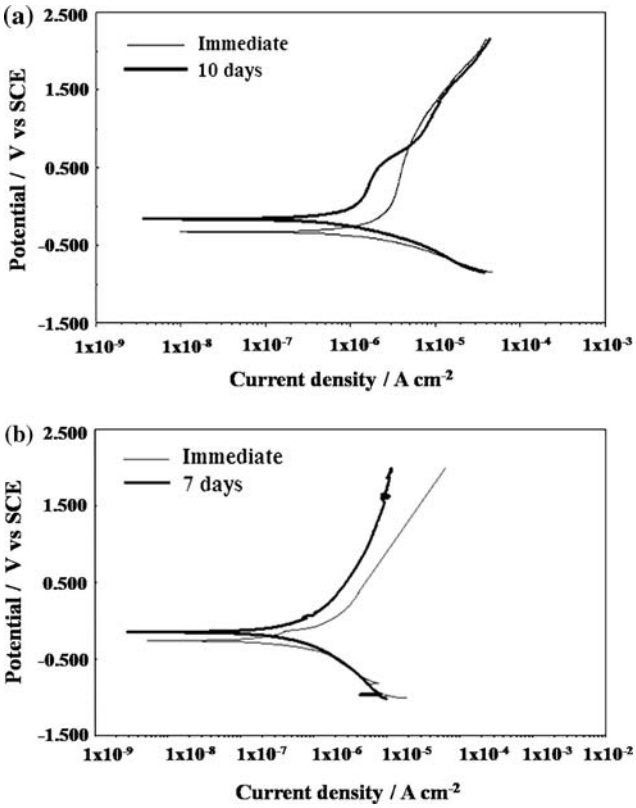

Fig. 3 Potentiodynamic polarization studies of Ti–6Al–4V ELI alloy in Hanks solution **a** AT and **b** AHT

Hanks solution. A higher current density was observed immediately after immersion, this behavior can be attributed to the porous nature of the surface, which facilitates dissolution of metals into the electrolyte [30]. However, after the 10th day of immersion, the current density was found to be lowered. This can be attributed to the formation of a protective layer over the porous layer or block in the pores of the layer present during immersion in SBF.

Figure 3b shows the polarization curves of AHT specimen for immediate and optimum day (7th) of immersion in

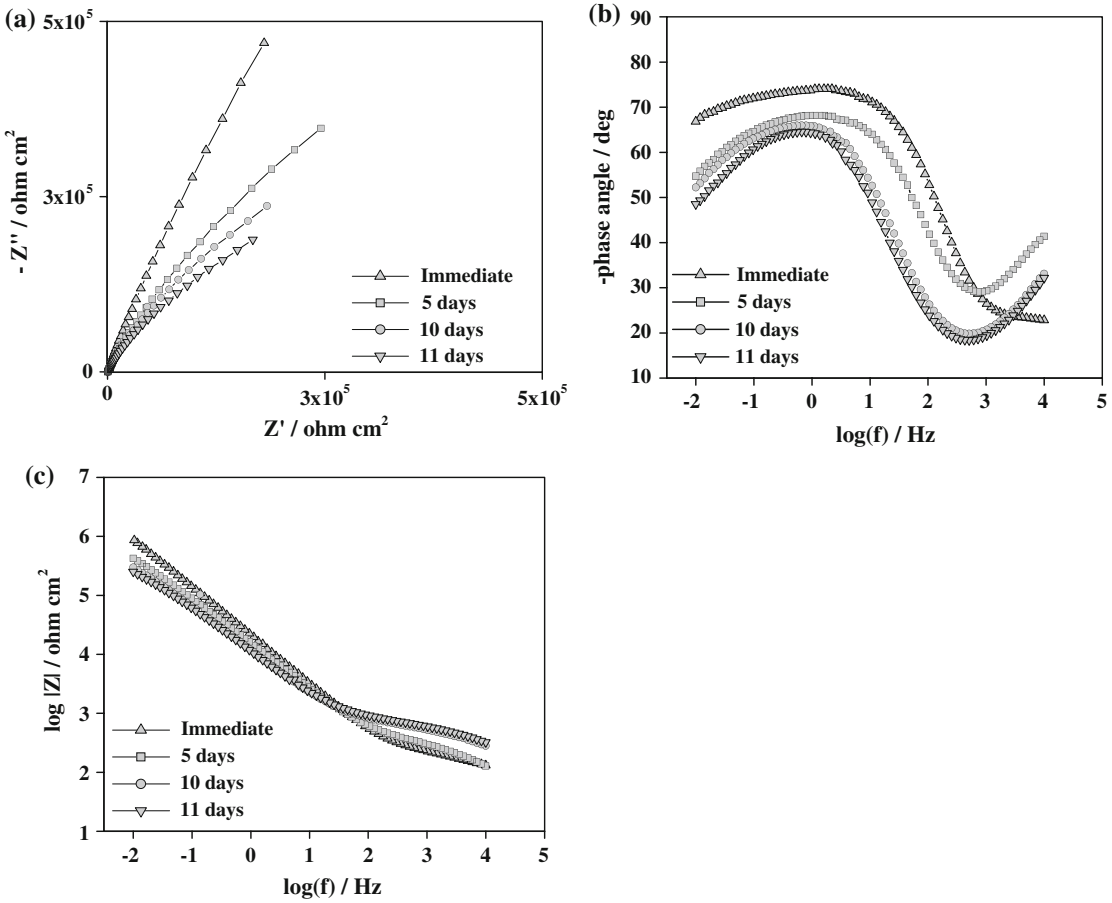

Fig. 4 Impedance spectrum of AT Ti–6Al–4V ELI alloy immersed in Hanks solution **a** Nyquist plot, **b** Bode phase angle and **c** Bode impedance plot

Hanks solution. In both the curves, the shift in current density due to oxygen evolution was not observed. This can be attributed to the densified porous film due to heat treatment. In addition, on the 7th day of immersion, a lower current density can be associated with a lower activity at metal–solution interface due to the formation of a compact passive film [31, 32].

3.2.2 EIS studies of alkali treated Ti–6Al–4V ELI alloy

The Nyquist plot (Fig. 4a) for different immersion periods in Hanks solution showed similar behavior. At low frequency region, very unique low magnitude phase angle behavior due to a new time constant was observed with increase in immersion period. The introduction of this new time constant at low frequency can be associated with the decrease in magnitude of the semi-infinite behavior, due to the interaction between electrode and electrolyte interface.

The Bode phase angle plots of AT Ti–6Al–4V ELI alloy immersed in Hanks solution for different durations are presented in Fig. 4b. Immediately after immersion, a single distinct capacitive behavior was observed. This was confirmed by a constant phase angle value of -70° at the intermediate and low frequency regions. As the immersion period increased, a shift in phase angle was observed at the high frequency region, the shift was apparently distinct on the 10th and 11th day of immersion. Further, the phase angle observed at the intermediate and low frequency regions was found to be at -60°.

Figure 4c shows the Bode impedance plots of AT alloy immersed in Hanks solution for different durations. It was observed that the solution resistance gradually increased with increase in immersion time. This observation indicated the decrease in free ions due to the adsorption of solution ions over the surface of the electrode, which in turn reflected on the conductivity of the solution.

The fitted Bode plot for AT alloy immersed in Hanks solution is shown in Figs. 5 and 6 show the equivalent circuit corresponding to the time of immersion. A single passive layer was denoted by R_s (R_gQ_g) for the passive film immediately after immersion whereas, a bilayer circuit viz., R_s (R_gQ_g) (R_bQ_b) for the 3rd day and R_s (R_aQ_a) (R_bQ_b) for 5th to 11th day of Ti–6Al–4V ELI alloy was proposed. The corresponding electrochemical impedance data

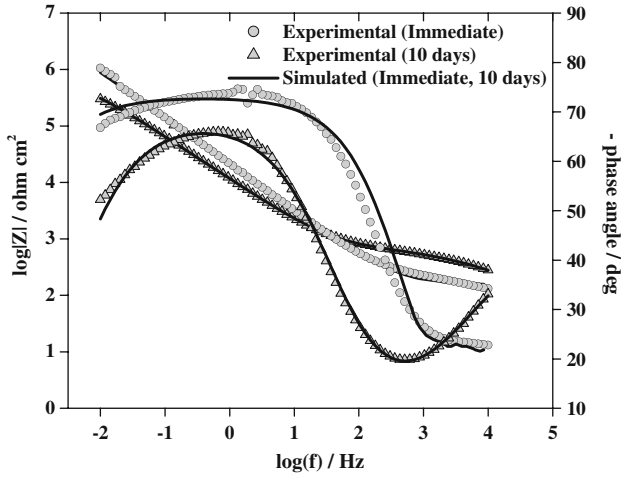

Fig. 5 Fitted Bode plot of AT Ti–6Al–4V ELI alloy immersed in Hanks solution

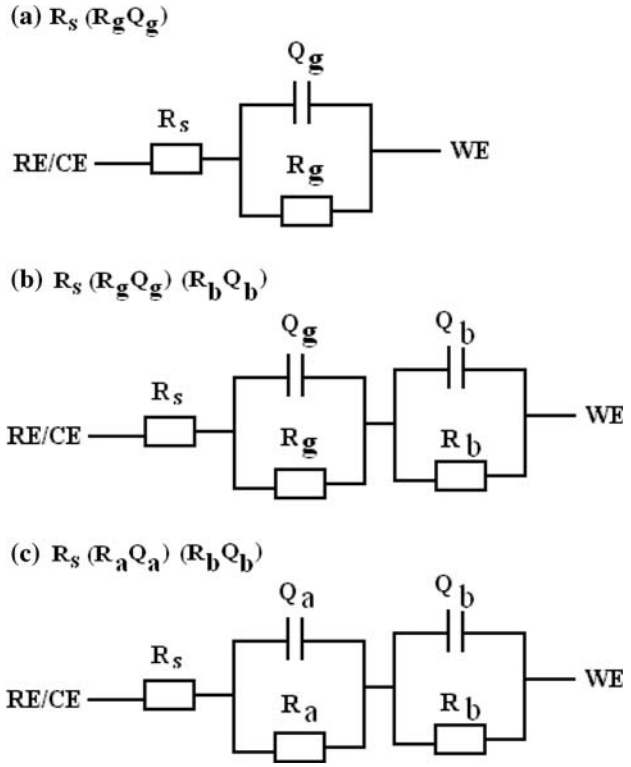

Fig. 6 Equivalent circuit diagrams for AT Ti–6Al–4V ELI alloy in Hanks solution **a** Immediate **b** 3 days and **c** 5–11 days

obtained by fitting models for different duration are presented in Table 1. These models were in good agreement with the impedance data obtained and the mechanism of apatite formation reported in literature [25, 33]. The high resistance observed immediately after immersion can be attributed to the presence of the gel layer formed after the alkali treatment. Further, the n_g values close to 1 evinced the ideal capacitance behavior of the gel layer. The continuous dissolution of gel layer and formation of barrier layer at the electrode/gel layer interface on the 3rd day of immersion can be understood from a lower Q_g, n_g, and R_g values. The formation of the barrier layer can be associated with the penetration of solution ions through the gel layer on to the surface of the metal.

Reports identify the formation of a compact oxide layer over the metal surface with exposure to solution ions [34]. The high R_b value indicated the high resistance of compact barrier layer. With further increase in the immersion period, the R_b value was found to be constant. The prolonged interaction of solution ions namely Ca^{2+} and PO_4^{3-} ions in the solution can be a cause for metamorphism in the gel layer to form a new CaP layer [32]. The low value of Q_a/R_a and n_a can be associated with the high porosity of Ca/P layer [35, 36].

3.2.3 *EIS studies of alkali heat-treated Ti–6Al–4V ELI alloy*

The Nyquist and Bode plots of AHT alloy at various durations (0th, 4th, 6th, and 7th day) in Hanks solution are shown in Fig. 7a, b. With immediate immersion, two distinct time constants were observed; the first one at higher frequency in the form of an incomplete semicircle and a second in the form of semi-infinite straight line. On the 4th day of immersion, only the semi-infinite line with a slight deviation in the angle of inclination was observed. On the 7th and 8th day of immersion, the plots were similar and exhibited three distinct time constants at higher frequency, at intermediate frequency and at lower frequency regions.

The phase angle plots of AHT Ti–6Al–4V ELI alloy immersed in Hanks solution for various durations are shown in Fig. 7c. The phase angle plots on the immediate immersion exhibited two distinct behaviors and it attained a maximum value of –70°. The phase angle at the lowest frequency was –50°. With increase in the time of immersion, there was a significant phase shift. For instance, on the 4th day of immersion, the phase angle maximum at low frequency was observed at −40°.

On the 7th and 8th day of immersion, three distinct phase angle behaviors were observed at higher, intermediate, and at lower frequency regions. The presence of a semicircle at intermediate region evinced the presence of a sandwich layer between the barrier layer and the outer layer. In addition, an inclined 45° line at low frequency region can be associated with a diffusion process.

Figure 7d shows the Bode impedance plot of various period of immersion in Hanks solution. As the immersion period increased, the resistance of the surface layer decreased, which can be attributed to the diffusion of solution ions into the metal surface. The fitted Bode plots for AHT Ti–6Al–4V ELI alloy are shown in Fig. 8 and the

Table 1 Electrochemical impedance parameters of AT Ti–6Al–4V ELI alloy obtained by fitting R_s (Q_gR_g), R_s (Q_gR_g) (Q_bR_b), and R_s (Q_aR_a) (Q_bR_b) model for different duration of immersion in Hanks solution

R_s (R_gQ_g)							
Duration (Day)	R_s × ohm cm^2	Q_g × μF cm^{-2}		n_g	R_g × K ohm cm^2		
Immediate	42.72	2.55		0.81	3939.6		
R_s (R_gQ_g) (R_bQ_b)							
Duration (Days)	R_s × ohm cm^2	Q_g × μF cm^{-2}	n_g	R_g × ohm cm^2	Q_b × μF cm^{-2}	n_b	R_b × K ohm cm^2
3	21.85	0.078	0.71	1.82	2.42	0.79	392.1
R_s (R_aQ_a) (R_bQ_b)							
Duration (Days)	R_s × ohm cm^2	Q_a × μF cm^{-2}	n_a	R_a × K ohm cm^2	Q_b × μF cm^{-2}	n_b	R_b × K ohm cm^2
5	5.54	0.059	0.69	0.08	2.16	0.77	371.8
7	2.45	0.005	0.63	0.16	2.42	0.76	323.6
10	2.01	0.001	0.55	0.18	2.66	0.76	239.6
11	2.10	0.001	0.55	0.20	2.33	0.75	168.8

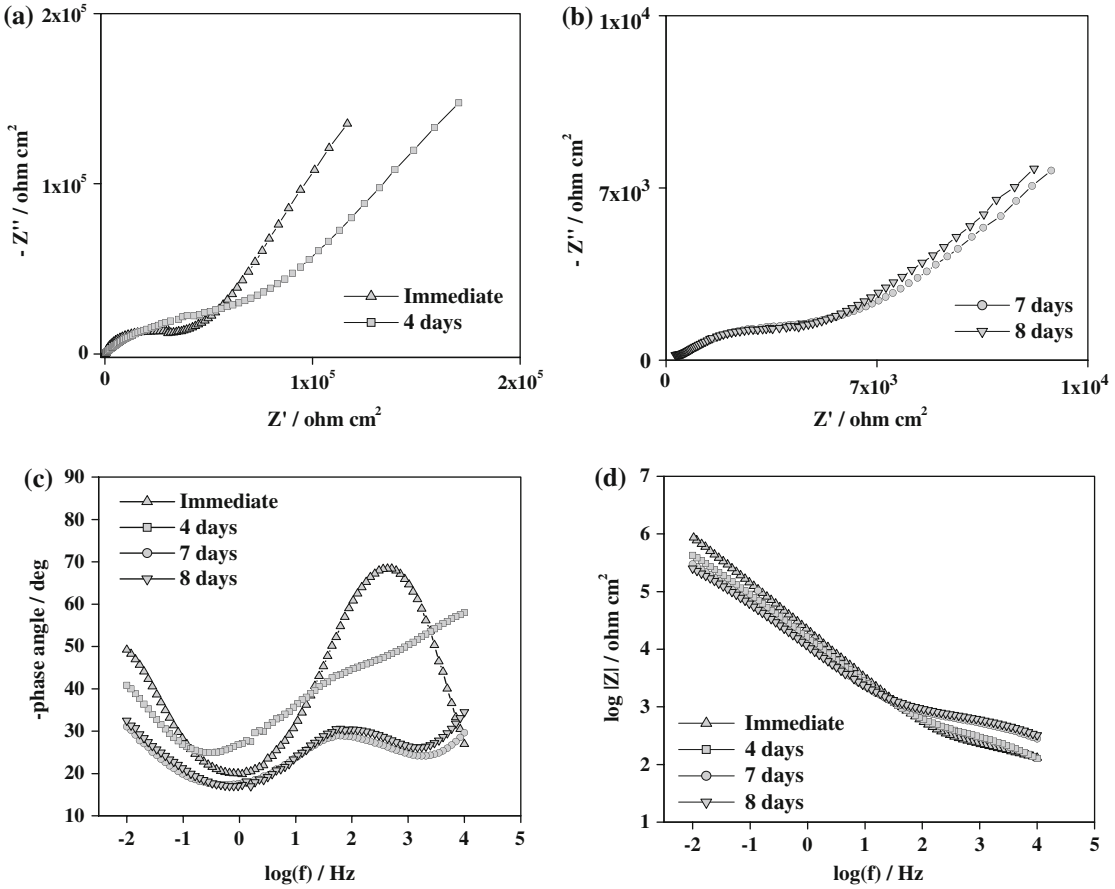

Fig. 7 Impedance spectrum of AHT Ti–6Al–4V ELI alloy immersed in Hanks solution **a** and **b** Nyquist plots, **c** Bode phase angle, and **d** Bode impedance plot

corresponding equivalent circuit model R_s (Q_a) (R_gQ_g) for immediate and 2nd day and R_s (W_a) (R_aQ_a) (R_bQ_b) for 4th to 8th day are shown in Fig. 9 and its electrochemical impedance data are given in Table 2. Immediately after immersion, the interaction of the solution ions leading to the formation of a layer is indicated as Q_a. The suffix 'a' represents the interaction of CaP over the densified gel layer. However, in the present context 'a' essentially does

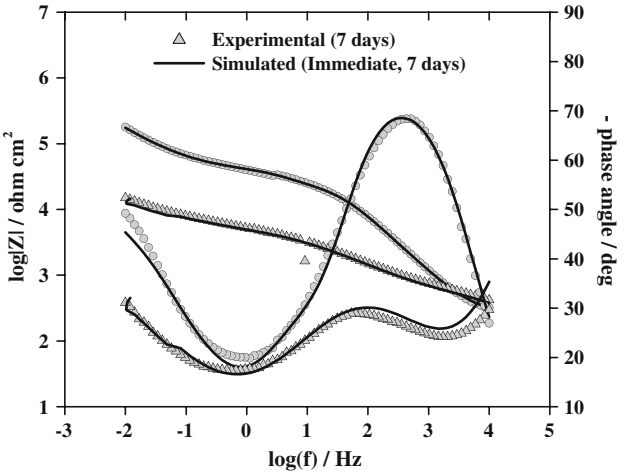

Fig. 8 Fitted Bode plot of AHT Ti–6Al–4V ELI alloy immersed in Hanks solution

not mean a fully grown apatite. The increase in Q_a value indicates a growing film. The decrease in the values of n_g, Q_g, and R_g indicates a metamorphism in the gel structure.

After 4 days of immersion, the capacitive behavior of the initially formed CaP layer transforms into a diffusive process over a porous layer. Hence, the electrical element Q_a transforms into a Warburg resistor (W_a), the decrease in the values of W_a with increase in immersion time can be associated with the penetration of the aggressive solution ions through the porous apatite layer and partially dissolved gel layer onto the surface of the metal and rendering a diffusion of the metal ions. Warburg diffusion in Ti–6Al–4V ELI has been attributed to V ions in earlier reports [37–40]. The decrease in the values of Q_g, n_g, and R_g indicates dissolution of the densified gel layer. The barrier layer of Ti–6Al–4V ELI alloy shows a tendency of thinning, indicated by the decrease in the values of Q_b, n_b, and R_b, the n_b attains a value of 0.5 which can be associated with a porous barrier layer unlike the reports of a compact barrier layer in Ti alloys. Since, it creates a vacancy in the oxide layer the barrier layer is destabilized [37]. Hence, the V ions present in the alloy are detrimental to the corrosion behavior of Ti–6Al–4V ELI alloy.

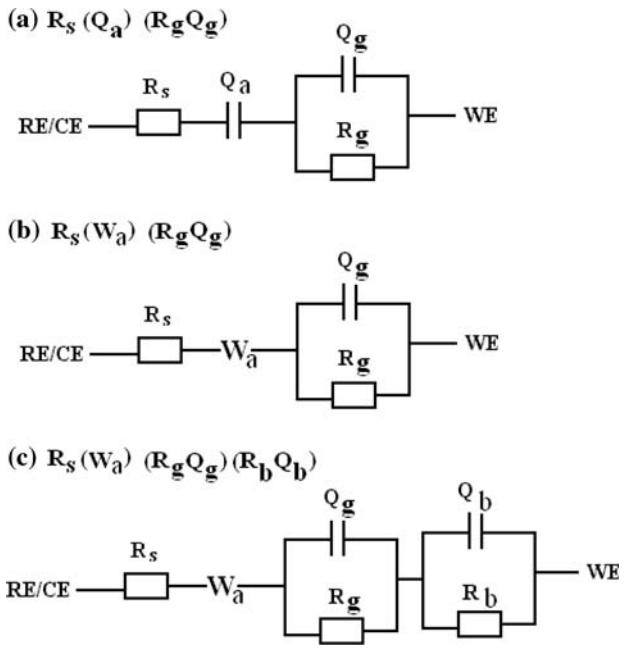

Fig. 9 Equivalent circuit diagrams for AHT Ti–6Al–4V ELI alloy in Hanks solution **a** Immediate–2 days and, **b** 4–8 days

4 Conclusions

The surface morphological and FT-IR spectroscopic results for AT and AHT specimens showed a uniform and well-defined porous network and the formation of densified gel layer over the surface. After the optimum period of immersion in Hanks solution, the data revealed a uniform coverage of apatite desiphered by the presence of Ca and P peaks in EDAX analysis. Potentiodynamic polarization results showed that the potential shifted significantly in the

Table 2 Electrochemical impedance parameters of AHT Ti–6Al–4V ELI alloy obtained by fitting R_s (Q_a) (Q_gR_g), R_s (W_a) (Q_gR_g), and R_s (W_a) (Q_gR_g) (Q_bR_b) model for different duration immersion in Hanks solution

R_s (Q_a) (R_gQ_g)								
Duration (Days)	R_s × ohm cm^2	Q_a × μF cm^{-2}	n_a	Q_g × μF cm^{-2}		n_g	R_g × K ohm cm^2	
Immediate	6.21	0.09	0.59	0.18		0.85	8.71	
2	5.96	0.28	0.58	0.10		0.79	10.47	
R_s (W_a) (R_gQ_g) (R_bQ_b								
Duration (Days)	R_s × ohm cm^2	W_a × 10^{-3} ohm cm^2	Q_g × μF cm^{-2}	n_g	R_g × K ohm cm^2	Q_b × μF cm^{-2}	n_b	R_b × K ohm cm^2
4	3.24	6.00	0.003	0.59	1.35	0.01	0.65	11.62
6	3.21	6.48	0.004	0.71	0.38	0.02	0.52	14.44
7	3.10	0.10	0.009	0.72	0.10	0.02	0.51	1.40
8	3.01	0.10	0.003	0.69	0.13	0.01	0.55	1.22

positive direction and the current density lowered due to the formation of an insulating layer over the surface. The impedance plot for AHT Ti–6Al–4V ELI alloy showed the presence of a bi-layered structure, with one of the layer being a thin film of TiO_2 and the other being the apatite layer, whereas, AHT specimen showed two distinct behavior along with the presence of Warburg diffusion impedance. The Warburg impedance was attributed to the diffusion of metal ions.

Acknowledgment The authors wish to thank Indian Council for Medical Research (ICMR), New Delhi for financial support of this research.

References

1. Leitao E, Silva RA, Barbosa MA (1997) Corros Sci 39:333
2. Elagli K, Traisnel M, Hildebrand HF (1993) Electrochim Acta 38:1769
3. Gonazalez JEG, Mirza Rosca JC (1999) J Electroanal Chem 471:109
4. Pan J, Thierry D, Leygraf C (1996) Electrochim Acta 41:1143
5. Turpin YL, Tardivel RD, Tallec A, Le Menn AC (2000) Dental Mater 16:57
6. Milosev I, Metikos-Hukovic M, Strehblow H-H (2000) Biomaterials 21:2103
7. Hench LL, Anderson O (1993) Bioactive glass coating. In: Hench LL, Wilson J (eds) An introduction to bioceramics. World Science Singapore, Singapore, p 239
8. Takatsuka K, Yamamuro T, Kitusgi T, Nakamura T, Shibuya T, Goto T (1993) J Appl Biomater 4:317
9. Groot KDE, Geeink RGT, Klein CPAT, Serekian P (1987) J Biomed Mater Res 21:1357
10. Yang CY, Lin RM, Wang BC, Lee TM, Chang E, Hang YS, Chen PQ (1997) J Biomed Mater Res 37:335
11. Ohtsuki C, Iida H, Hayakawa S, Osaka A (1997) J Biomed Mater Res 35:39
12. Li PJ, Groot KDE (1993) J Biomed Mater Res 27:1495
13. Wen HB, Wolke JGC, De Wijn JR, Liu Q, Cui FZ, Groot KDE (1997) Biomaterials 18:1471
14. Kokubo T, Miyaji F, Kim HM (1996) J Am Ceram Soc 79:1127
15. Wen-Fu HO, Chien-Hung Lai, Hsueh-Chuan Hsu, Shih-Ching Wu (2009) Surf Coating Technol 203:3142
16. Faure J, Balamurugan A, Benhayoune H, Torres P, Balossier G, Ferreira JMF (2009) Mater Sci Eng C 29:1252
17. Jianyu Xiong, Yuncang Li, Xiaojian Wang, Peter Hodgson, Cui'e Wen (2008) Acta Biomaterialia 4:1963
18. Daqing Wei, Yu Zhou, Yuanbin Wang, Qingchang Meng, Dechang Jia (2008) Surf Coating Technol 202:5012
19. Raman V, Tamilselvi S, Rajendran N, Rajendran N (2007) Electrochimica Acta 52:7418
20. Jianjui Xie, Ben Li Luan (2008) J Mater Sci Mater Med 19:3211
21. Rakngarm Achariya, Miyashita Yukio, Mutoh Yoshiharu (2008) J Mater Sci Mater Med 19:1953
22. Ciobanu Gabriela, Carja Gabriela, Sandu Octavian Ciobanu Ion, Sandu Andrei (2009) Micron 40:143
23. Chen Dianying, Jordan Eric H, Gell Maurice, Wei Mei (2008) Acta Biomaterialia 4:553
24. Tamilselvi S, Raman V, Rajendran N (2006) Electrochim Acta 52:839
25. Wang CX, Wan M, Zhou X (2003) Biomaterials 24:3069
26. Liang F, Zhou L, Wang K (2003) Surf Coating Technol 165:133
27. Liang F, Zhou L, Wang K (2003) J Mater Sci Lett 22:1665
28. Lin FH, Hsu YS, Lin SH, Chen TM (2004) Mater Chem Phy 87:24
29. Kim HM, Miyaji F, Kokubo T, Nakamura T (1996) J Biomed Mater Res 32:409
30. Ghicov A, Tsuchiya H, Macak MJ, Schmuki P (2005) Electrochem Commun 7:505
31. Frauchiger L, Taborelly M, Aronsson BO, Descounts P (1999) Appl Surf Sci 143:67
32. Yang BC, Weng J, Li XD, Zhang XD (1999) J Biomed Mater Res 47:213
33. Wang CX, Wang M (2002) Mater Lett 54:30
34. Jonasova L, Muller FA, Helebrant A, Strnad J, Greil P (2004) Biomaterials 25:1187
35. Shukla AK, Balasubramaniam R (2005) Corros Sci 48:1696
36. Silva TM, Rito JE, Simoes AMP, Ferreira MGS, Belo Cunha DAM, Watkins KG (1998) Electrochim Acta 43:203
37. Marinovic A, Metilos-Hukovic M, Baratac G, Gojo M (eds) (2001) II Croatian symposium on electrochemistry. In: Proceedings of the Croatian society of chemists and chemical engineers, vol 2. Zagreb, p 123
38. Aziz-Kerrzo M, Conroy KG, Fenelon AM, Farrell ST, Breslin CB (2001) Biomaterials 22:1531
39. Leito E, Barbosa MA, KGe Groot (1995) J Mater Sci Mater Med 9:543
40. Hanawa T, Ota M (1991) Biomaterials 12:767